Available online at www.sciencedirect.com
SCIENCE DIRECT
Wear 261 (2006) 172–179
WEAR
www.elsevier.com/locate/wear

# Rolling contact fatigue resistance of ductile iron with different nodule counts and matrix microstructures

R.C. Dommarco *, A.J. Jaureguiberry, J.A. Sikora

*Grupo Tribología, Div. Metalurgia, INTEMA, Universidad Nacional de Mar del Plata, Av.J.B. Justo 4302, B 7608 FDQ Mar del Plata, Argentina*

Received 11 February 2005; received in revised form 26 August 2005; accepted 22 September 2005
Available online 27 October 2005

**Abstract**

Thin wall ductile iron castings are being used in the industry as a way to improve the strength to weight ratio of machine parts. The high cooling rate, suffered by thin wall parts during the solidification process, promotes several microstructural changes, such as, carbide precipitation and a noticeable nodule count increment. The present work, studies the effect that the increase in nodule count has on the rolling contact fatigue resistance of ductile iron with different matrix microstructures. Ductile cast iron test samples, with nodule counts ranging between 150 and 1400 nod/mm$^2$ were obtained. The samples were then heat treated in order to obtain three sets of different ADI grades and also a quenched and tempered set. The rolling contact fatigue properties were evaluated by using a flat washer type test rig. Different relations of the contact area versus the nodule size were obtained by using three different counterparts. The results show that an increase in the nodule count promotes a noticeable increase in the rolling contact fatigue life, being more important for the quenched and tempered samples. The relation between contact area surface and nodule size was the main variable influencing the rolling contact fatigue life.


*Keywords:* Ductile iron; Thin wall; Nodule count; Rolling contact; Contact area size; Nodule size

## 1. Introduction

The use of ductile iron (DI) has increased constantly since its introduction in the market in the 1950s, due to its excellent mechanical properties and low production costs. Subsequently, the development of the austempered ductile iron (ADI) in the 1970s produced a new and important impulse for the application of DI, thanks to the excellent combination of strength and toughness of this emerging material.

Nowadays, the development of DI has introduced thin-walled ductile iron (TWDI) as a new improvement, in order to increase the strength to weight ratio and, in consequence, its competitiveness against light alloys.

The high cooling rate taking place during solidification of thin wall ductile iron castings, promotes two main changes in the microstructure: (a) the precipitation of iron carbides and (b) an important increase in the nodule count. The use of thin walls (less than 4 mm thickness) can increase the nodule count up to 2000 nod/mm$^2$ [1,2].

Furthermore, the resulting finer structure decreases the distance for carbon diffusion and increases the amount of graphite-matrix interfaces. This, in turn, would also reduce micro-segregation and could modify the kinetics of solid-state transformation during heat treatments [3]. The literature shows that a moderate increase in nodule count in normal wall parts, from 100 to 250 nod/mm$^2$, increases the strength and ductility, due to a finer and more homogeneous microstructure obtained by austempering [4].

The research work carried out up to the present has been mainly orientated to improve the castability of thin wall parts, to prevent casting defects, to avoid carbide precipitation or to optimize carbide dissolution [2,5,6]. Some studies have already shown that samples obtained from 3 mm thickness plates in the "as cast" condition have higher tensile strength than those obtained from 12 mm thickness [7,8].

In a previous work, it was observed that the increase in nodule count produces an important increase in the RCF resistance of DI [9]. Two important examples of the use of DI in machine elements, subjected to rolling contact loading, are gears and cams. The observed results may have an important impact for this type of parts since it is possible to control the nodule count by

* Corresponding author. Tel.: +54 223 481 6600x245; fax: +54 223 481 0046.
*E-mail address:* dommarco@fi.mdp.edu.ar (R.C. Dommarco).

0043-1648/$ – see front matter © 2005 Published by Elsevier B.V.
doi:10.1016/j.wear.2005.09.015

two different ways. One of them is by controlling the inoculation process and the other one is by using chills in the mold, which not necessary promote carbides precipitation if the chemical composition is correctly controlled.

The present work focuses on the study of the influence of nodule count and nodule size on the RCF resistance of TWDI with different nodule count levels. Also, the influence of different matrices and contact areas were evaluated.

## 2. Experimental procedure

### 2.1. Sample preparation and microstructural analysis

Two ductile iron heats were obtained in a metal casting laboratory facility, using a 55 kg capacity medium frequency induction furnace and regular quality raw materials. Inoculation and nodulization procedures were carried out in a ladle with nodulization pocket, by using conventional techniques. The chemical composition of the heat was determined by means of a Baird Spark Emission Optic Spectrograph with a DV6 excitation source.

Three kinds of RCF samples, with noticeable differences in nodule count, were obtained. Samples with a nodule count considered as "normal" (NNC) were machined from a 70 mm diameter and 350 mm length bar, cast in a sand mold. Due to geometrical requirements of the RCF test rig, the high cooling rates typical of thin-walled parts, were simulated in the lab by using a mold with a copper chill in the bottom, in order to obtain the high nodule count samples (HNC) on the surface to be tested [9,10]. The opposite side of these samples has an intermediate or medium nodule count (MNC) and were also used to evaluate the influence of nodule count on the RCF life.

After rough machining, according to the details given in Fig. 1, some of the RCF samples were heat treated by austempering while the remaining were quenched and tempered (Q&T) according to the heat treatment parameters listed in Table 1. Then, the samples were finished by grinding and polishing the surfaces to be tested. Quenched and tempered SAE 4140 steel samples were also evaluated, and their characteristic lives were used as reference values.

Metallographic samples were prepared by using standard techniques. Metallographic etching was performed with 2% Nital. The nodularity and nodule count values were measured by using both, the ASTM A 247 standard and the Image Pro Plus software. Worn surfaces were studied by using optical and scanning electron microscopes.

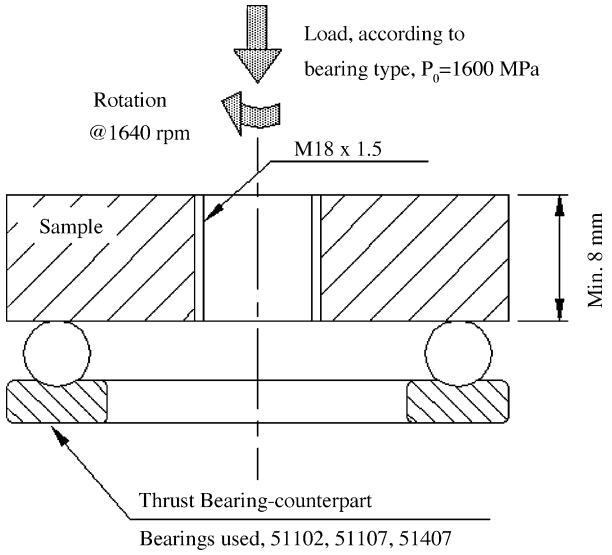


Fig. 1. Scheme of the washer type rolling contact fatigue tester machine, showing sample geometry and dimensions, load, speed and the bearing types used as a counterpart.

### 2.2. Rolling contact fatigue tests

The RCF tests were carried out in a flat washer type tester [11]. The RCF testing rig was modified by introducing two new counterparts in order to obtain three different contact area sizes and evaluate the RCF life at different "contact area versus nodule area size (Ca/Ns)" relations. The test sample, shown in Fig. 1, rotates at 1640 rpm leading to different loading frequencies, depending on the bearing type used, as listed in Table 2. Testing conditions were selected to produce the microasperities interaction, i.e. a lubricant film thickness factor $\lambda < 1$. Even though contact conditions were not ideal, maximum contact stress, $p_0$, and oil film thickness, $h_0$, were calculated as reference values only, by using the Hamrock and Brewe [12] and the Hamrock and Dowson [13] solutions, respectively. The contact load was selected to reach a pressure $p_0 \approx 1600$ MPa at each ball independently of the bearing type or size. According to the Hertzian (elastic) theory, this pressure produces a circular contact patch between the sample and the ball, having different diameters for each bearing type as listed in Table 2.

The specimens were loaded until failure, i.e. spalling took place and the test was automatically stopped once a certain vibration level was detected by an accelerometer. Six tests were carried out for each material variant. The RCF tests results were analyzed using the two-parameter Weibull statistic, and the $L_{10}$,

Table 1
Heat treatment parameters for austempering and quenching and tempering

| Heat | Heat treatment | Austenitizing temperature (°C) | Austempering temperature (°C) | Tempering temperature (°C) | Hardness (HRC) | Sample identify |
|---|---|---|---|---|---|---|
| #1 | Austempering | 910 | 360 | | 38 | ADI 360 |
| #1 | Austempering | 910 | 260 | | 48 | ADI 260 |
| #1 | Quenching + tempering | 880 | | 200 | 54 | Q&T |
| #2 | Austempering | 910 | 240 | | 49 | ADI 240 |
| SAE 4140 | Quenching + tempering | 850 | | 240 | 50 | SAE 4140 |

Table 2
Characteristic parameters used for the RCF tests, depending on the bearing type used as a counterpart. Cd/Nd stands for the relation between contact diameter and nodule diameter

| Bearing type | Ball diameter (mm) | Load per ball (N) | Hertz press (MPa) | Contact diameter (mm) | Loading cycles/h |
|---|---|---|---|---|---|
| 51102 | 4 | 11 | 1612 | 0.114 | 636500 |
| 51107 | 6 | 18 | 1625 | 0.146 | 842900 |
| 51406 | 12 | 97 | 1620 | 0.339 | 524400 |

$L_{50}$ and $\eta$ (medium) lives were evaluated. Rolling direction (RD) was defined as opposite to the direction of sample rotation.

## 3. Results and discussion

### 3.1. Samples characterization

Table 3 lists the chemical composition of the heats used, showing slightly hypereutectic equivalent carbon. A high silicon level, as typically used in TWDI, was employed to improve graphitization under the high cooling rates imposed by the chill. The small percentage of carbides precipitated during solidification was fully dissolved during the austenitizing step of the ADI heat treatment [6].

For heat #1, the nodule count values for the normal nodule count (NNC) sand cast samples was ~150 nod/mm$^2$, while for the high nodule count (HNC) samples was ~1000 nod/mm$^2$. For heat #2, the nodule counts were ~300 nod/mm$^2$ for NNC samples, 600 nod/mm$^2$ for the MNC samples and ~1400 nod/mm$^2$ for HNC samples with maximum nodule count diameters of ~15, ~20 and ~60 μm, respectively. Fig. 2 shows the unetched metallographies for all the samples types of heat #2.

The hardness of the different austempered and Q&T samples is listed in Table 1.

### 3.2. Rolling contact fatigue tests

#### 3.2.1. Results for heat #1 samples

Based on previous tests [9], the comparison in RCF resistance between NNC and HNC samples was extended to both, the samples austempered at 360 °C and the quenched and tempered samples.

The life values of the different RCF tests were processed by means of the Weibull statistics and the "failure probability (%) versus life to failure (loading cycles)" relationships were obtained. Fig. 3 shows the results for the iron samples and also for the Q&T SAE 4140 steel used as a reference material. Fig. 3(a) shows the results for the samples austempered at 360 °C, for both "normal" (ADI 360 NNC) and "high" (ADI 360 HNC) nodule counts and also the reference material. Fig. 3(b) shows the results obtained for the samples austempered at 260 °C (ADI 260 NNC and ADI 260 HNC) [9] and the SAE 4140, while Fig. 3(c) shows the results for the Q&T ductile iron with normal and high nodule counts (Q&T NNC and Q&T HNC). Table 4 lists the characteristic values for the plots of Fig. 3, such as: $L_{10}$, $L_{50}$, and medium ($\eta$) lives, and also the characteristic slope—$\beta$ and the correlation factor—$r^2$, which fall between the typical values for RCF tests.

Table 3
Chemical composition [wt.%] of the heats used for the RCF samples. CE = carbon equivalent. Balance, Fe

| Sample | C | Si | Mn | S | P | Mg | CE |
|---|---|---|---|---|---|---|---|
| Heat #1 | 3.48 | 2.80 | 0.38 | <0.02 | <0.06 | 0.04 | 4.42 |
| Heat #2 | 3.20 | 3.35 | 0.19 | 0.034 | 0.037 | 0.04 | 4.34 |

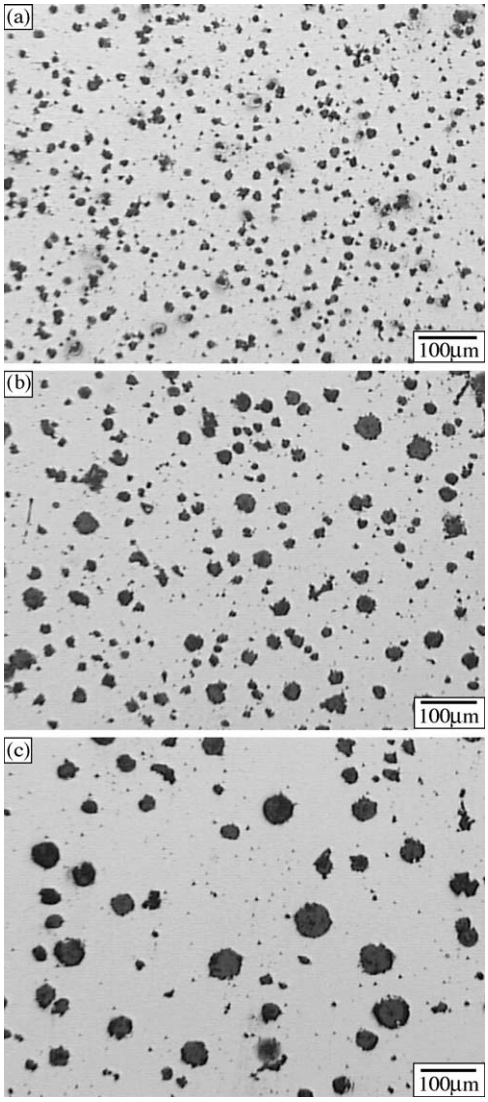


Fig. 2. Unetched microstructures of heat #2 showing the differences in nodule count for: (a) high nodule count (HNC), (b) medium nodule count (MNC) and (c) normal nodule count (NNC) samples.

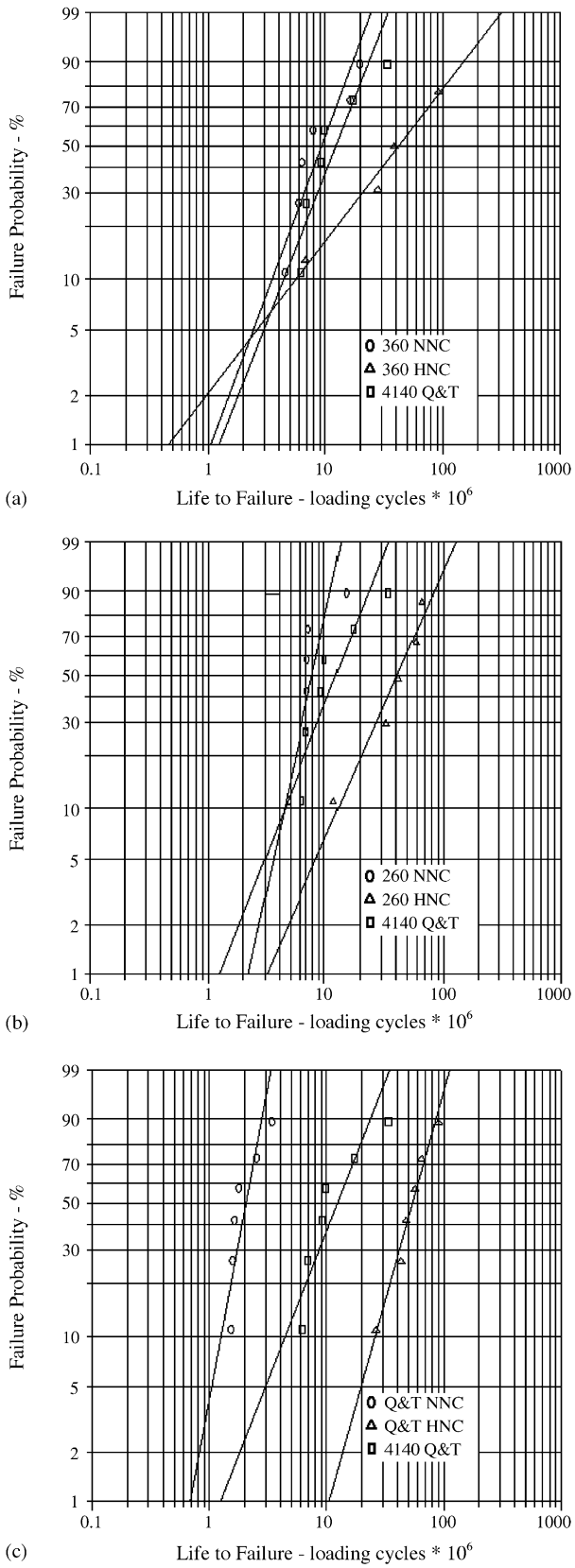


Fig. 3. Rolling contact fatigue lives for heat #1 samples: (a) ADI 360 samples for NNC and HNC variants, (b) ADI 260 samples for NNC and HNC and (c) for the Q&T NNC and HNC variants. Q&T SAE 4140 steel was used as a reference material.

The results clearly show an important increase in the RCF lives as the nodule count of the samples increases. As a reference value for this increment Table 4 also lists the relations between the medium life ($\eta$) of the HNC and NNC sample sets for each material variant.

As it was speculated earlier, the "contact area surface versus nodule size (Cs/Ns)" relation was the main variable influencing the results, as an important RCF lives increment was observed, even though the microstructures were changed. Then, an adaptation of the RCF test rig was made and a second ductile iron heat was prepared, in order to be able to evaluate the RCF resistance of the DI variants at different Cs/Ns relationships.

### 3.2.2. *Results for heat #2 samples*

This heat was used firstly to evaluate the influence of different contact area sizes and secondly to verify the trends on the influence of nodule count. The first objective was reached by modifying the test rig to accommodate three different counterparts, i.e. the standard 51107 type thrust bearing and the 51102 and 51407 types. Fig. 4 shows the nodule sizes for the HNC, MNC and NNC samples and the different contact area corresponding to the three bearing types used, clearly showing the comparative size relations. All the "contact area diameter versus nodule diameter (Cd/Nd)" and "contact area surface versus nodule size (Cs/Ns)" relations are listed in Table 5.

Fig. 5(a) shows the plots corresponding to the ADI 240 NNC, tested with the three different counterparts, i.e. the 51102, 51107 and 51406 bearing types, showing that the RCF life increases as the contact area size increases. Fig. 5(b) shows a similar plot, but in this case for the ADI 240 HNC samples, also indicating that the increase in contact area promotes an increase in the RCF life.

Fig. 5(c) shows the results obtained for the different nodule counts of heat #2, including those corresponding to the MNC samples, i.e. with a nodule count of ~600 nod/mm$^2$. In this case, the 51107-thrust bearing was the same in all cases. Again, a strong influence of the nodule size and/or the Cs/Ns relation on the RCF life was observed and evidenced by the increase in

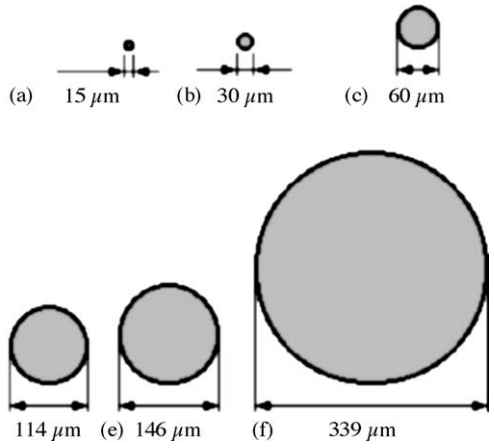


Fig. 4. Representation of the nodule and contact area sizes for the HNC, MNC and NNC samples and for the contact areas obtained with the 51102, 51107 and 51406 bearing types at the same contact pressure, $p_0 \approx 1600$ MPa.

Table 4
Characteristic values of the Weibull plots obtained for heat #1 RCF tests

| Sample | $L_{10}$ life | $L_{50}$ life | $\eta$-Medium life | β-Characteristic life | $r^2$-Correlation factor | $\eta_{HNC}/\eta_{NNC}$ |
|---|---|---|---|---|---|---|
| 260 NNC | 4.389 | 7.730 | 8.630 | 3.328 | 0.703 | 5.85 |
| 260 HNC | 12.90 | 40.46 | 50.54 | 1.648 | 0.950 | |
| 360 NNC | 3.535 | 9.308 | 11.23 | 1.945 | 0.845 | 5.58 |
| 360 HNC | 5.658 | 42.22 | 62.42 | 0.967 | 0.977 | |
| T&R NNC | 1.257 | 2.047 | 2.250 | 3.864 | 0.724 | 27.6 |
| T&R HNC | 25.98 | 53.88 | 62.10 | 2.5820 | 0.978 | |
| 4140 Q&T | 4.434 | 12.32 | 15.03 | 1.843 | 0.809 | 1 |

Table 5
"Contact area diameter vs. nodule diameter (Cd/Nd)" and "Contact area surface vs. nodule size (Cs/Ns)" relations for all the sample and thrust bearing combinations

| Bearing type | Cd/Nd for NNC | Cd/Nd for MNC | Cd/Nd for HNC | Cs/Ns for NNC | Cs/Ns for MNC | Cs/Ns for HNC |
|---|---|---|---|---|---|---|
| 51102 | 1.9 | 3.8 | 7.6 | 3.6 | 14.1 | 57.6 |
| 51107 | 2.4 | 4.8 | 9.7 | 5.9 | 22.5 | 95.6 |
| 51406 | 5.6 | 11.3 | 22.6 | 31.9 | 126.7 | 510 |

the RCF life when the nodule count or the Cs/Ns increase (see Table 5, row 2, columns 5–7). The characteristic values for the plots of Fig. 4 are summarized in Table 6.

### 3.2.3. Analysis of the RCF wear tracks

The wear tracks were analyzed by using a scanning electron microscope. Fig. 6(a) shows details of the exit side of a spall corresponding to an ADI 240 NNC sample as a result of a test carried out with the 51102 bearing type. A network of cracks connecting nodules and delineating portions of material about to be detached are visible. In Fig. 6(b), a wider wear track produced by the 51406 bearing type is observed with a similar failure appearance showing a crack network along the wear track edge where maximum tensile stresses take place.

Fig. 7(a) shows the bottom of the spall in an ADI 240 HNC sample. The presence of nodules at the crack surface is evident at higher magnification, Fig. 7(b). As it was reported [14,15], a crack propagating in an ADI structure follows a path connecting nodules and this results in a higher nodule count at the surface crack than in the flat polished condition.

## 3.3. Discussion

Taking into account the lives obtained for the NNC samples, indicated in Fig. 5(a) and listed in Table 6, it is observed that the medium lives relations such as $\eta_{51107}/\eta_{51102}$ and $\eta_{51406}/\eta_{51102}$ were 1.67 and 19.78, respectively. The contact area size relations, $Cs_{51107}/Cs_{51102}$ and $Cs_{51406}/Cs_{51102}$ were 1.67 and 8.85, respectively. On the other hand, the contact area diameter relations, $Cd_{51107}/Cd_{51102}$ and $Cd_{51406}/Cd_{51102}$ were 1.28 and 2.97, respectively. Then, it is possible to conclude that the medium lives relations are closer to the contact area size relations, rather than to the contact area diameter relations.

Fig. 8 shows a similar analysis in a bar graph extended to all the nodule count and bearing type combinations used (including those corresponding to MNC samples), with their corresponding medium lives ($\eta$). First bar for each combination shows the increase of the diameter relation while the second bar shows the increase in the area relation. The third bar shows how the medium life increases as either the diameter or the area relations' increase.

The results obtained by changing the counterpart in tests were the nodule count was maintained constant; confirm the experimental evidence obtained when the contact area was hold constant and the nodule count was changed. Therefore, when the Cs/Ns increases the RCF life strongly increases for the relations evaluated in the present work, as shown in Fig. 3 for heat #1. The same trends were observed for the DI samples of heat #2, as shown in the Weibull plots of Fig. 5, in this case also introducing the contact area as a variable.

Cast irons with free graphite can be considered as composites. In such case, this material would be a composite of a particular type, since the presence of the second phase, the graphite, on one side yields the improvements of many properties such as

Table 6
Characteristic values of the Weibull plots obtained for heat #2 RCF tests. BT, bearing type

| Sample | $L_{10}$ life | $L_{50}$ life | $\eta$-Medium life | $\beta$-Slope | $r^2$-Correlation factor | $\eta_{HNC}/\eta_{NNC}$ |
|---|---|---|---|---|---|---|
| 240 NNC 51102 BT | 0.700 | 1.812 | 2.181 | 1.981 | 0.634 | 7.36 |
| 240 HNC 51102 BT | 3.626 | 12.61 | 16.07 | 1.511 | 0.946 | |
| 240 NNC 51107 BT | 0.889 | 2.908 | 3.661 | 1.590 | 0.957 | 5.68 |
| 240 HNC 51107 BT | 7.736 | 17.57 | 20.81 | 2.169 | 0.881 | |
| 240 NNC 51406 BT | 21.61 | 38.53 | 43.12 | 3.256 | 0.888 | 5.91 |
| 240 HNC 51406 BT | 105.5 | 220.7 | 254.7 | 2.553 | 0.942 | |
| 240 MNC 51107 BT | 2.249 | 3.838 | 4.259 | 3.523 | 0.954 | |

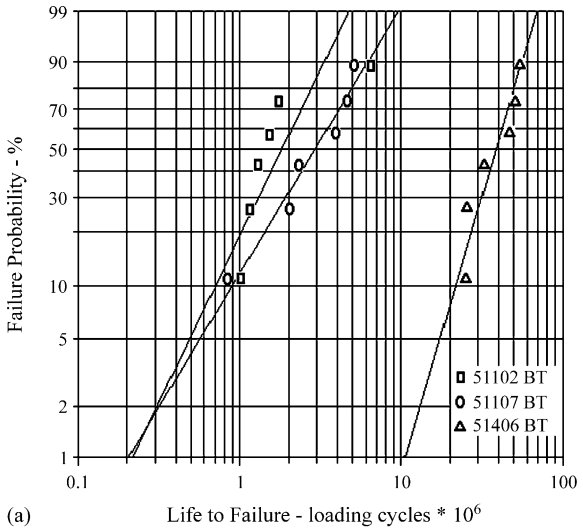


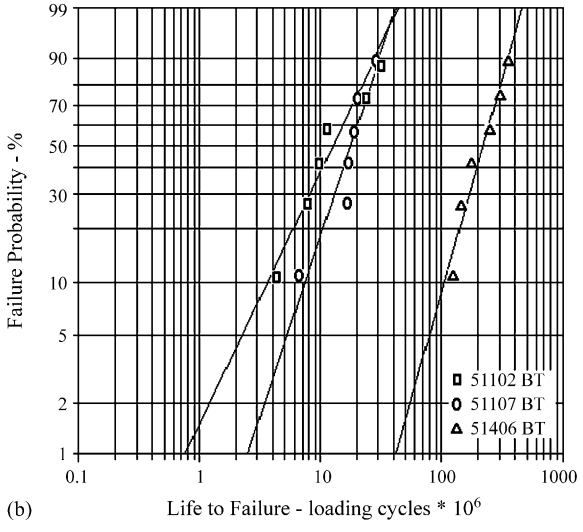


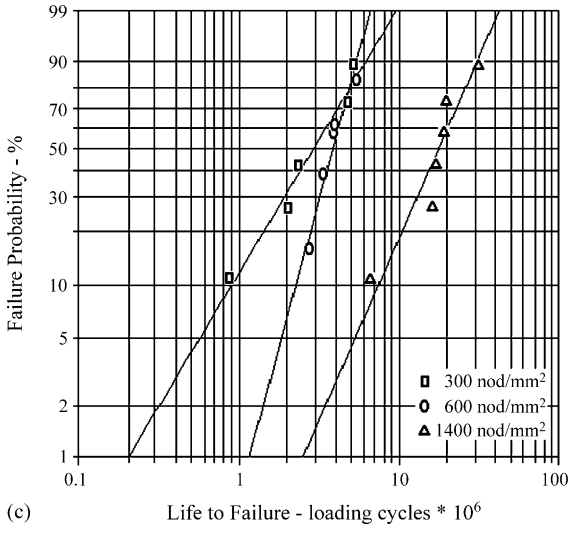


Fig. 5. Rolling contact fatigue lives for heat #2 samples: (a) NNC samples (∼300 nod/mm$^2$) and different bearing types, (b) HNC samples (∼1400 nod/mm$^2$) and different bearing types and (c) different nodule counts with 51107 bearing type.

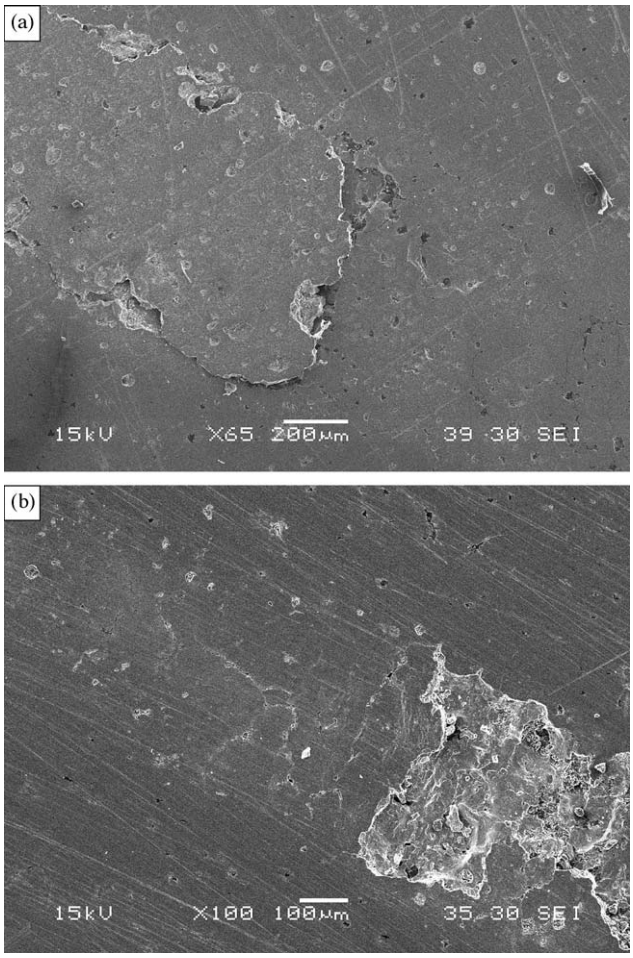


Fig. 6. Spalls in ADI 240 NNC samples: (a) with a 51102 bearing type as a counterpart and (b) with a 51406 bearing type as a counterpart. Rolling direction is from right to left.

contraction during solidification, machinability, friction, thermal conductivity, dumping capacity, etc. Nevertheless, on the other side, graphite certainly impairs mechanical properties such as strength, toughness, fatigue and also the wear resistance, due to its very low strength. In the case of fatigue graphite acts as a defect, in particular for rolling contact fatigue due to the interaction with the rolling element. The interaction of a rolling element (in this study represented by the balls of the counterpart) and any discontinuity on the wear track (in this case a graphite nodule) was already studied [16–20], clearly showing the detrimental effect of the defects presence. In particular, a 2-D numerical model [21] for the case in which a defect of width $b$ is in the center of a contact area of width $a$ has shown that the ideal contact pressure distribution ($p$) with a maximum contact pressure ($p_0$) is modified, having two pressure spikes right at the edge of the discontinuity, with values much higher than $p_0$. The study was carried out for several relations between ($b$) and ($a$), showing that the pressure spikes increase as ($b$) increases. Therefore, considering the graphite nodules as defects on the wear track, the pressure spikes in NNC samples will be higher than those in MNC samples, and these in turn, will be higher than those in HNC samples. In this case, the decrease in the pressure spikes

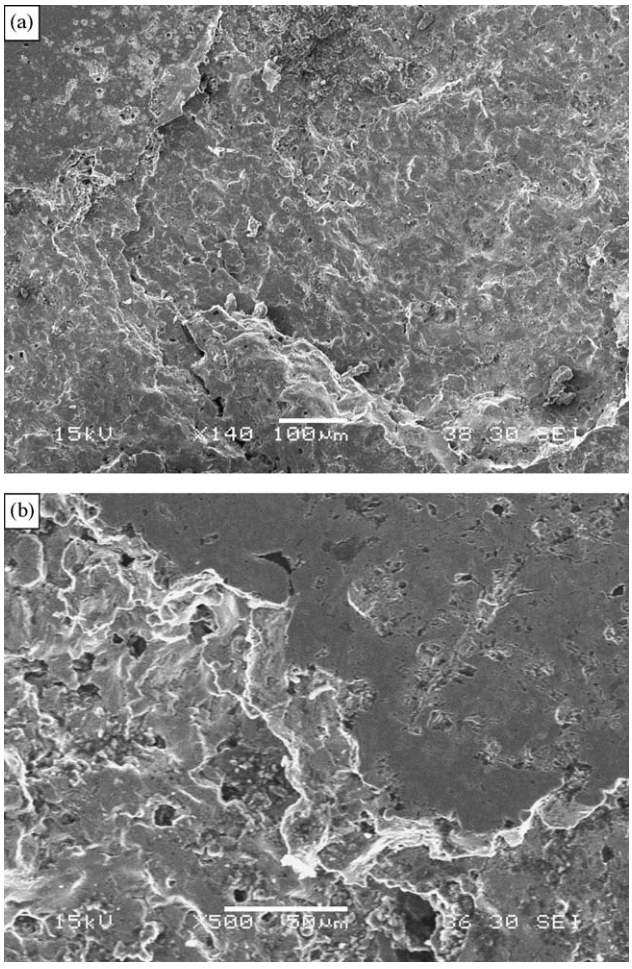


Fig. 7. Spalls in ADI 240 HNC samples for different counterparts: (a) with a 51102 bearing type and (b) with a 51406 bearing type. Rolling direction is from right to left.

has certainly overcome the increase in the number of defects or nodules acting as crack nucleation sites as it was also demonstrated in a previous work [9].

The theories predicting the life to failure under fatigue conditions, either in bending fatigue or rolling contact fatigue [22,23], depend on the stress level (i.e., on the possibility of producing the critical amount of plasticity for crack nucleation). Therefore, predicting fatigue life by using theories applied to the calculated pressure spikes will coincide with the present results.

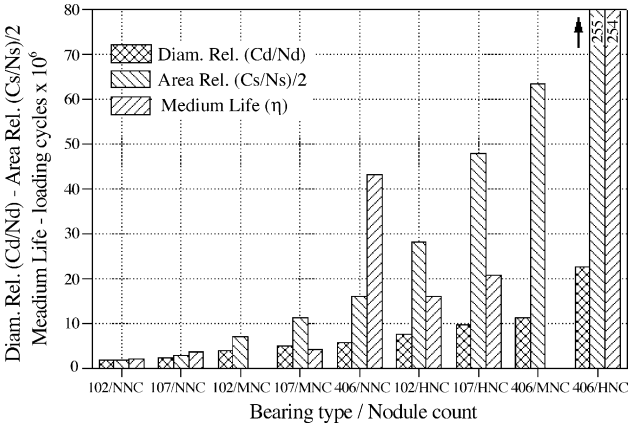


Fig. 8. Bar diagram showing the increase in contact area, nodule area and medium life for the different bearing type and material variant combinations.

The RCF tests results for different microstructures have shown that the strong increment in the RCF life when shifting from NNC to HNC. ADI is a consequence of the stress levels originated by the geometrical differences of defects and balls, rather than changes in the material matrix.

The results of the present work are encouraging in terms of being able to modify the RCF life of conventional thickness DI castings, by increasing the nodule count through inoculation. Nevertheless, there is no inoculation method capable to produce an increase of the nodule count higher than 100%.

## 4. Conclusions

The RCF testing procedure was modified in order to gain the possibility of testing with different contact areas by using different types of thrust bearings as a counterpart and, at the same time, maintaining constant the maximum contact pressure. Also, different nodule counts were obtained employing different solidification rates, allowing to study the influence of nodule size on the RCF resistance at different "contact area size versus nodule size (Cs/Ns)".

The results show that the nodule size affects the RCF life independently of the ductile iron microstructure, with a strong RCF life increment for the case of the quenched and tempered variant when the nodule size decreases.

The RCF resistance is strongly affected by changes in the nodule size, but it can be also improved by the increase in the contact area, as it was demonstrated by testing with different contact areas sizes, while the nodule size was maintained constant.

## References

[1] R. Ruxanda, L. Beltran-Sanchez, J. Massone, D.M. Stefanescu, On the eutectic solidification of spheroidal graphite iron—an experimental and mathematical modelling approach, AFS Trans. 109 (2001) 1037–1047.
[2] L. Achour, M. Martínez Gamba, R. Boeri, J. Sikora, Determinación de parámetros de colada para la obtención de pequeños espesores en fundición de grafito esferoidal, in: Proceedings of the SAM 2000 Congress, Neuquén, Argentina, August 2000, pp. 115–122.
[3] J. Massone, R. Boeri, J. Sikora, Solid state transformation kinetics of high nodule count ductile iron, Int. J. Cast Met. Res., 16 (2003) 1–3, 251–256.
[4] G. Cooper, A. Roebuck, Hamid Bayati, R. Elliott, The influence of nodule count on the austempering kinetics of a Mn–Cu ductile iron, Int. J. Cast Met. Res. 11 (1999) 227–235.
[5] A. Javaid, J. Thomson, M. Sahoo, K. Davis, Factors affecting the formation of carbides in thin wall DI castings, AFS Trans. 107 (1999) 441–456.
[6] A. Giacopini, R. Boeri, J. Sikora, Carbide dissolution in thin walled ductile iron, Mat. Sci. Technol. 19 (12) (2003) 1755–1760.
[7] L. Achour, M. Martínez Gamba, R. Boeri, J. Sikora, Thin wall ductile iron castings: characterization of the microstructure, in: Proceedings of the IBEROMET VI Congress, Barcelona, Spain, 2000, pp. 419–426.
[8] A. Javaid, K.G. Davis, M. Sahoo, Effect of chemistry and processing variables on mechanical properties of thin wall DI castings, AFS Trans. 108 (2000) 191–200.

[9] N. Rebasa, R. Dommarco, J. Sikora, Wear resistance of high nodule count ductile iron, Wear 253 (2002) 855–863.
[10] R. Dommarco, J. Salvande, Contact fatigue resistance of austempered and partially chilled ductile irons, Wear 254 (2003) 230–236.
[11] P. Moens, M. Teutónico, R. Dommarco, Desarrollo de un equipo para evaluar la resistencia a la fatiga de contacto por rodadura, in: Proceedings of the SAM 2000 Congress, Neuquén, Argentina, August 2000, pp. 435–442.
[12] B. Hamrock, Brewe, Simplified solution for stresses and deformation, J. Lubric. Technol. 105 (1983) 171.
[13] B. Hamrock, D. Dowson, Isothermal elasto-hydrodynamic lubrication of point contacts. Part III—fully flooded results, J. Lubric. Tech. (Trans. ASME) 99 (1997) 264–276.
[14] R. Dommarco, P. Bastias, H. Dall'O, G. Hahn, C. Rubin, Rolling contact fatigue (RCF) resistance of austempered ductile iron (ADI), Wear 221 (1998) 69–74.
[15] G. Greno, J. Otegui, R. Boeri, Mechanism of fatigue crack growth in austempered ductile iron, Int. J. Fatigue 21 (1999) 35–43.
[16] W. Holzhauer, Surface changes around large raceway indentations during run-in of tapered roller bearings, Tribol. Trans. 34 (3) (1991) 361–368.
[17] W. Cheng, H.S. Cheng, L.M. Keer, Experimental investigation on rolling/sliding contact fatigue crack initiation with artificial defects, Tribol. Trans. 37 (1) (1994) 1–12.
[18] P. Bastias, G. Hahn, C. Rubin, V. Gupta, X. Leng, Analysis of rolling contact spall life in 440 C bearing steel, Wear 171 (1994) 169–178.
[19] R. Dommarco, Resistencia a la fatiga de contacto por rodadura. Degradación y falla superficial, PhD Thesis, School of Engineering, INTEMA, Nat. Univ. Mar del Plata, Argentina, Noviembre 1977.
[20] D. Nélias, F. Ville, Detrimental effects of debris dents on rolling contact fatigue, J. Tribol. 122 (2000) 55–64.
[21] V. Gupta, G. Hahn, P. Bastias, C. Rubin, Influence of indent geometry on repeated two-dimensional rolling contact, J. Tribol. 117 (1995) 655–659.
[22] G. Lundberg, A. Palmgren, Dynamic capacity of roller bearings, Acta Polytech. M.E. Series 2 (1952) 4.
[23] E. Ionnides, T. Harris, A new fatigue life model for rolling bearings, J. Tribol. (Trans. ASME) 107 (1985) 367–378.